# Analysis of Coplanar-Waveguide Discontinuities with Finite-Metallization Thickness and Nonrectangular Edge Profile

Fang-Lih Lin and Ruey-Beei Wu, *Member, IEEE*

***Abstract*— In this paper, the hybrid finite-element method (FEM) is proposed to analyze the coplanar-waveguide (CPW) discontinuities with finite-metallization thickness. A variational formula for the electric field in the slot region between upper and lower half-space is derived by applying the variational-reaction theory and solved by the FEM. In the limiting case of zero metallization thickness, this finite-element analysis is reduced to a moment-method analysis using Galerkin's approach with rooftop basis functions. The edge profile effects of a trapezoidal slot cross resulting from the etching or sputtering process can also be easily considered by this approach. Some numerical results are presented for short- and open-ended CPW discontinuities for different conductor thicknesses. It has been shown that not only the metallization thickness, but also the conductor-edge profile, can produce noticeable effects on circuit performance and should be taken into account for accurately modeling the CPW discontinuities.**

***Index Terms*— Coplanar waveguides (CPW's), finite-element method (FEM), transmission-line discontinuities.**

## I. Introduction

THE uniplanar transmission-line structure based on the coplanar waveguide (CPW) has been developed as a circuit element for monolithic microwave integrated circuits (MMIC's). Accurate analysis and characterization of CPW discontinuity is important in designing the MMIC because tuning or trimming of MMIC's is infeasible. As the line size in the metallization plane shrinks, the finite-metallization thickness may play a significant role in determining the circuit performance and should be taken into account.

Several papers have been presented to characterize shielded CPW discontinuity structures with finite-metallization thickness based on the mode-matching technique [1]–[3], the transverse resonance technique (TRT) [4], [5], or the finite-difference method in frequency domain [6]. In applying these methods, the structures to be analyzed must be closed by the electric or magnetic walls and, hence, the radiation effects cannot be accounted for. On the other hand, Tran *et al.* [7] utilized the extended spectral-domain approach to analyze the unshielded CPW discontinuities with finite-metallization thickness. This method needs to compute the field patterns of uniform CPW lines on both sides of discontinuities in advance, which is by itself a considerable task.

All the methods mentioned above only dealt with slots of rectangular cross section. In practice, the cross section of the strip is likely to be better approximated by a trapezoid than by a rectangle due to the nonideal underetching or electrolytical growth in the integrated circuit (IC) manufacturing process. Recent studies have shown that not only the finite-metallization thickness, but also the conductor-edge profile will affect the electrical characteristics of uniform microstrip [8]–[12] and CPW lines [13], [14]. It is then necessary to account for the effects of conductor-edge profile for accurately modeling the CPW discontinuities.

For this purpose, the finite-element method (FEM) hybridized with suitable integral equations for the exterior field was utilized to calculate the capacitance or inductance of CPW discontinuities with finite metallization in the quasi-static approximation [15], [16]. However, the full-wave analysis is required to account for the high-frequency effects. In this paper, a variational formula in terms of the electric field in the slot region is derived in Section II. The effects of surface- and space-wave radiation are included in the integral-equation formulation by the Green's functions for the exterior field. The variational formula is solved in Section III by applying the FEM with edge vector elements as the basis functions. In the limiting case of zero thickness, the formula reduces to an integral equation which is commonly employed in the moment-method analysis. Section IV presents some numerical results for the short- and open-ended discontinuities with finite-metallization thickness. Effects of conductor-edge profile are considered in Section V. Finally, brief conclusions are drawn in Section VI.

## II. Variational-Reaction Formulation

The cross section of a CPW with finite-metallization thickness is shown in Fig. 1(a). The solution region $\Omega$ lies between the upper and lower slot surfaces, denoted by $S_u$ and $S_l$, respectively. The variational equation for the unknown electric field in $\Omega$ can be derived by applying the variational-reaction theory [17], [18]. First, consider the reaction form

$$\delta\Psi = \iiint_{\Omega} (\delta\overline{E} \cdot \overline{J})\, d\Omega = 0 \tag{1}$$

Manuscript received December 9, 1996; revised May 26, 1997. This work was supported in part by the National Science Council, Republic of China, under Grant NSC86-2221-E002-043.

The authors are with the Department of Electrical Engineering, National Taiwan University, Taipei, Taiwan 10617, R.O.C.

Publisher Item Identifier S 0018-9480(97)08246-X.

where $\delta\overline{E}$ is an arbitrary test field and $\overline{J}$ is the trial source supporting the trial field $(\overline{E}, \overline{H})$ with the relation

$$\overline{J} = \nabla \times \overline{H} - j\omega\epsilon_0 \overline{E}. \tag{2}$$

Substituting (2) into (1) and employing vector identities, the reaction form becomes

$$\begin{aligned}\delta\Psi &= \iiint_{\Omega} (\delta\overline{E} \cdot \nabla \times \overline{H} - j\omega\epsilon_0\, \delta\overline{E} \cdot \overline{E})\, d\Omega \\ &= \sum_{p=u,\,l} \iint_{S_p} (\hat{n}_p \cdot \overline{H} \times \delta\overline{E})\, ds \\ &\quad + \iiint_{\Omega} (\overline{H} \cdot \nabla \times \delta\overline{E} - j\omega\epsilon_0\, \delta\overline{E} \cdot \overline{E})\, d\Omega \end{aligned} \tag{3}$$

where $\hat{n}_p$ $(p = u$ or $l)$ is the unit vector outward normal to slot surface $S_p$.

Then, using $\overline{E}$ formulation, the magnetic field $\overline{H}$ in (3) is expressed in terms of the trial electric field, i.e.,

$$\overline{H} = -\frac{1}{j\omega\mu_0} \nabla \times \overline{E} \tag{4}$$

inside $\Omega$ by the Maxwell's equation and (5), shown at the bottom of the page, by employing the proper Green's function described in [19]. Here, $\overline{H}^{\text{inc}}$ denotes the magnetic field of the incident wave.

Substituting (4) and (5) into (3) yields the following desired variation equation:

$$\begin{aligned}\delta\Psi' &= 0 \\ \Psi' &= -\frac{\Psi}{j\omega\epsilon_0} \\ &= \frac{1}{2} \iiint_{\Omega} \left( \overline{E} \cdot \overline{E} - \frac{1}{k^2} \nabla \times \overline{E} \cdot \nabla \times \overline{E} \right) d\Omega \\ &\quad + \sum_{p=u,\,l} \tfrac{1}{2} \iint_{S_p} \iint_{S_p} \hat{n}_p \times \overline{E}(\overline{R}) \cdot \overline{\overline{G}}_p \cdot \hat{n}_p \\ &\quad \times \overline{E}(\overline{R}')\, ds'\, ds \\ &\quad + \frac{1}{j\omega\epsilon_0} \iint_{S_u} \overline{H}^{\text{inc}} \cdot \hat{n}_u \times \overline{E}(\overline{R})\, ds. \end{aligned} \tag{6}$$

It is not difficult to show that the equation is stationary at the exact electric field.

## III. Finite-Element Analysis

### A. Contributions of the Interior Fields

The FEM is employed to solve the variational equation (6). The solution region $\Omega$ is divided into a number of small-volume elements. In case of rectangular cross section, the element can be chosen as a simple rectangular brick shown in Fig. 1(b). By using the vector basis functions, the field within each element is expanded as

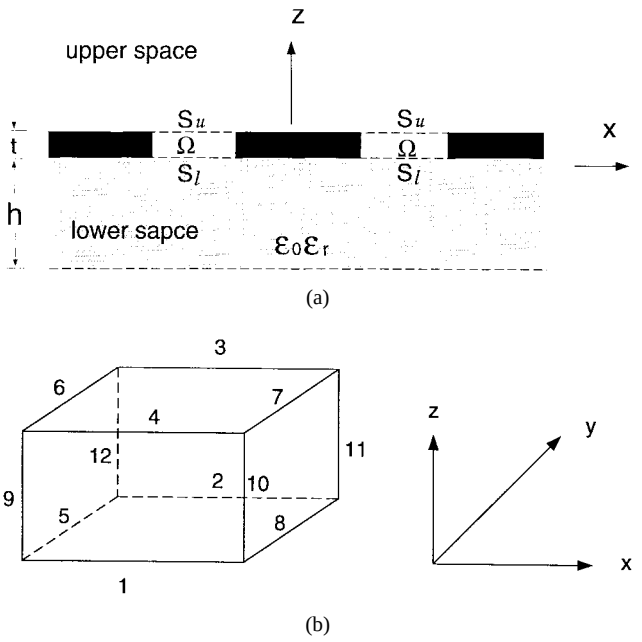


Fig. 1. (a) The cross-sectional geometry of the CPW with metallization thickness $t$ and (b) rectangular brick edge element.

$$\overline{E}^e(\overline{R}) = \sum_{i=1}^{12} E_i^{(e)} \overline{B}_i(\overline{R}) \tag{7}$$

where $E_i^{(e)}$'s denote the average tangential electric fields along the edge $i$ of the $e$th element $\Omega_e$, and $\overline{B}_i$'s the corresponding vector basis functions [20]. Substituting (7) into (6), the volume integral in (6) becomes

$$\begin{aligned}&\iiint_{\Omega} \left( \overline{E} \cdot \overline{E} - \frac{1}{k^2} \nabla \times \overline{E} \cdot \nabla \times \overline{E} \right) d\Omega \\ &\quad = \sum_{e} \left\{ \sum_{i=1}^{12} \sum_{j=1}^{12} E_i^{(e)} E_j^{(e)} \left[ M_{ij}^{(e)} - \frac{1}{k^2} N_{ij}^{(e)} \right] \right\} \end{aligned} \tag{8}$$

where

$$\begin{aligned} M_{ij}^{(e)} &= \iiint_{\Omega_e} \overline{B}_i(\overline{R}) \cdot \overline{B}_j(\overline{R})\, d\Omega \\ N_{ij}^{(e)} &= \iiint_{\Omega_e} \nabla \times \overline{B}_i(\overline{R}) \cdot \nabla \times \overline{B}_j(\overline{R})\, d\Omega. \end{aligned}$$

### B. Contributions of the Boundary Fields

Due to the discretization in the interior region, the slot surfaces are divided accordingly into a number of small surface patches. On the boundary surfaces $S_u$ and $S_l$, $\overline{B}_i(\overline{R})$ in (7)

$$\overline{H} = \begin{cases} \overline{H}^{inc} + j\omega\epsilon_0 \displaystyle\iint_{S_u} \overline{\overline{G}}_u(\overline{R}, \overline{R}') \cdot \hat{n}_u \times \overline{E}(\overline{R}')\, ds', & \text{on } S_u \\ j\omega\epsilon_0 \displaystyle\iint_{S_l} \overline{\overline{G}}_l(\overline{R}, \overline{R}') \cdot \hat{n}_l \times \overline{E}(\overline{R}')\, ds', & \text{on } S_l \end{cases} \tag{5}$$

becomes a rooftop basis function along the $\hat{x}$- or $\hat{y}$-direction. The surface field can be expanded as

$$\hat{n} \times \overline{E}^s = \sum_{i=1}^{N_s} E_i^s \overline{\Lambda}_i(\overline{R}) \tag{9}$$

where $\overline{\Lambda}_i = \hat{n} \times \overline{B}_i^s$ and $N_s$ is the number of expansion terms. The surface integrals in (6) can be written as

$$\iint_{S_p} \iint_{S_p} \hat{n}_p \times \overline{E}(\overline{R}) \cdot \overline{\overline{G}}_p \cdot \hat{n}_p \times \overline{E}(\overline{R}') \, ds' \, ds = \sum_{i=1}^{N_s} \sum_{j=1}^{N_s} E_i^{(S_p)} E_j^{(S_p)} Y_{ij}^{(S_p)}, \qquad p = u \text{ or } l \tag{10}$$

and

$$\frac{1}{j\omega\epsilon_0} \iint_{S_u} \overline{H}^{\text{inc}}(\overline{R}) \cdot \hat{n}_u \times \overline{E}(\overline{R}) \, ds = \sum_{i=1}^{N_s} h_i^{\text{inc}} E_i^{(S_u)}. \tag{11}$$

Here, $E_i^{(S_p)}$'s are the edge unknowns on the slot surface $S_p$. The coefficients $Y_{ij}^{(S_p)}$ ($p = u$ or $l$) and $h_i^{\text{inc}}$ are given by

$$Y_{ij}^{(S_p)} = \iint_{S_p} \iint_{S_p} \Lambda_i(w) \hat{w} \cdot \overline{\overline{G}}_p(\overline{R}, \overline{R}') \cdot \hat{w}' \, \Lambda_j(w') \, ds' \, ds \tag{12}$$

$$h_i^{\text{inc}} = \frac{1}{j\omega\epsilon_0} \iint_{S_u} H_w^{\text{inc}} \, \Lambda_i(w) \, ds \tag{13}$$

where $\hat{w}$ and $\hat{w}'$ are in the $\hat{x}$- or $\hat{y}$-direction.

Assembling the terms from all the elements, (6) is discretized into a matrix form

$$\begin{aligned} \Psi' &= \frac{1}{2} \sum_e \left\{ \sum_{i=1}^{12} \sum_{j=1}^{12} E_i^{(e)} E_j^{(e)} \left[ M_{ij}^{(e)} - \frac{1}{k^2} N_{ij}^{(e)} \right] \right\} \\ &\quad + \frac{1}{2} \sum_{p=u,\,l} \sum_{i=1}^{N_s} \sum_{j=1}^{N_s} E_i^{(S_p)} E_j^{(S_p)} Y_{ij}^{(S_p)} - \sum_{i=1}^{N_s} h_i^{\text{inc}} E_i^{(S_u)} \\ &= \frac{1}{2} [E]^T [G][E] - [E]^T [h^{\text{inc}}] \end{aligned} \tag{14}$$

where $[E]$ is a column vector consisting of all the edge unknowns, and the superscript $T$ stands for vector transpose. Application of the Rayleigh–Ritz procedure to (14) yields a system of simultaneous equation

$$[G][E] = [h^{\text{inc}}] \tag{15}$$

which can be readily solved by the Gaussian elimination method.

Given the electric fields on the slot surface, the matrix pencil approach is then utilized to extract the scattering coefficients and from which, the normalized impedance and admittance of the CPW discontinuities. Detailed excitation scheme and extraction procedure can be referred to [19].

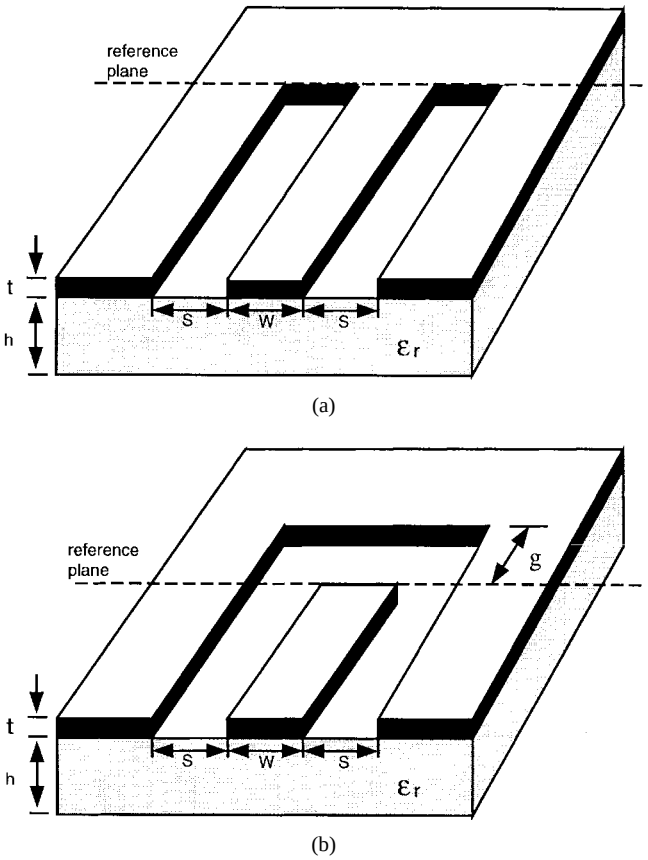


Fig. 2. The CPW discontinuity structures. (a) Short end. (b) Open end.

### C. Zero Metallization-Thickness Case

In the limiting case that the metallization thickness is negligible, the terms $M_{ij}^{(e)}$ and $N_{ij}^{(e)}$ in (14) tend to zero. The boundary surfaces $S_u$ and $S_l$ coincide with each other and as a result $E_i^{(S_u)} = E_i^{(S_l)} = E_i$. The matrix equation in (14) can be reduced to

$$[Y^{(S_u)} + Y^{(S_l)}][E] = [h^{\text{inc}}] \tag{16}$$

where the vector $[E]$ includes only the edge unknowns on the slot surface, i.e.,

$$[E] = [E_1, E_2, \cdots, E_{N_s}]^T.$$

A moment-method analysis has already been presented to deal with CPW discontinuity with zero metallization thickness [19]. The resultant equation (14) obtained by the present analysis is based on the same integral equation and employs the same rooftop function $\Lambda(w)$ as the basis. In other words, the special treatment required in the efficient numerical evaluation of the surface integral [19, eq. (12)] applies here.

## IV. Numerical Results and Discussion

A number of analyses for CPW with finite-metallization thickness have been made, including both the effective dielectric constant and end effects. The discontinuities to be considered are short- and open-ended structures, shown in Fig. 2. Unless otherwise specified, the line parameters are chosen as follows: $w = 20$ $\mu$m, $s = 15$ $\mu$m, $t = 3$ $\mu$m,

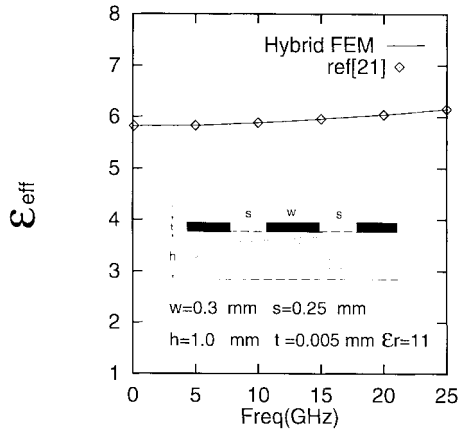


Fig. 3. Comparison of the effective dielectric constants of the CPW calculated by the present method with those given in [21].

$h = 200$ $\mu$m, and $\epsilon_r = 12.9$ for which the CPW line has a characteristic impedance of about 50 $\Omega$ on GaAs substrate. The gap width of the CPW open end is $g = 15$ $\mu$m.

In the numerical computation, the metallization thickness $t$ is modeled by one division cell since it is usually smaller than those of the conductor and slot widths in a typical MMIC structure. In the $x$–$y$ plane, the uniform CPW line section is chosen to be three-and-one-half wavelength long, as required by the matrix-pencil approach [19]. The number of division cells in the longitudinal direction is about 40 per wavelength. Nonuniform division is applied on the region near the discontinuity end.

Along the transverse direction, the slot width is divided into $N = 1$ or 2 cells. It is found that the relative error of the resultant effective dielectric constant for $N = 1$ and $N = 2$ is only about 0.27%. For the ended effect, the maximum relative error of the equivalent length extension is about 2.3% at 100 GHz for the short-ended discontinuity. For simplicity, the slot width is divided into one cell in the following analysis, which assumes a uniform slot field distribution in the transverse direction. The total numbers of unknowns are about 650 for short end and 700 for open end, respectively. The computation time per frequency point is about 23 min for short end and 27 min for open end on a Sun Sparc station 20 with 96 Mbytes RAM.

Being developed mainly for the CPW discontinuities, the present approach can obtain the characteristics of the associated uniform CPW lines as by-products. For example, consider a CPW short-end structure with line parameters following those employed in [21]. Fig. 3 shows the effective dielectric constants of the CPW line extracted from the calculated fields of the CPW short end. The results are compared with the data published in [21] and good agreement can be found between them.

Fig. 4(a) and (b) show the effective dielectric constants and the normalized resistances and reactances of a CPW short end with metallization thickness $t = 0$ and 3 $\mu$m as a parameter. Here, the normalized impedance is calculated from

$$z = r + jx = \frac{1 + S_{11}}{1 - S_{11}} \tag{17}$$

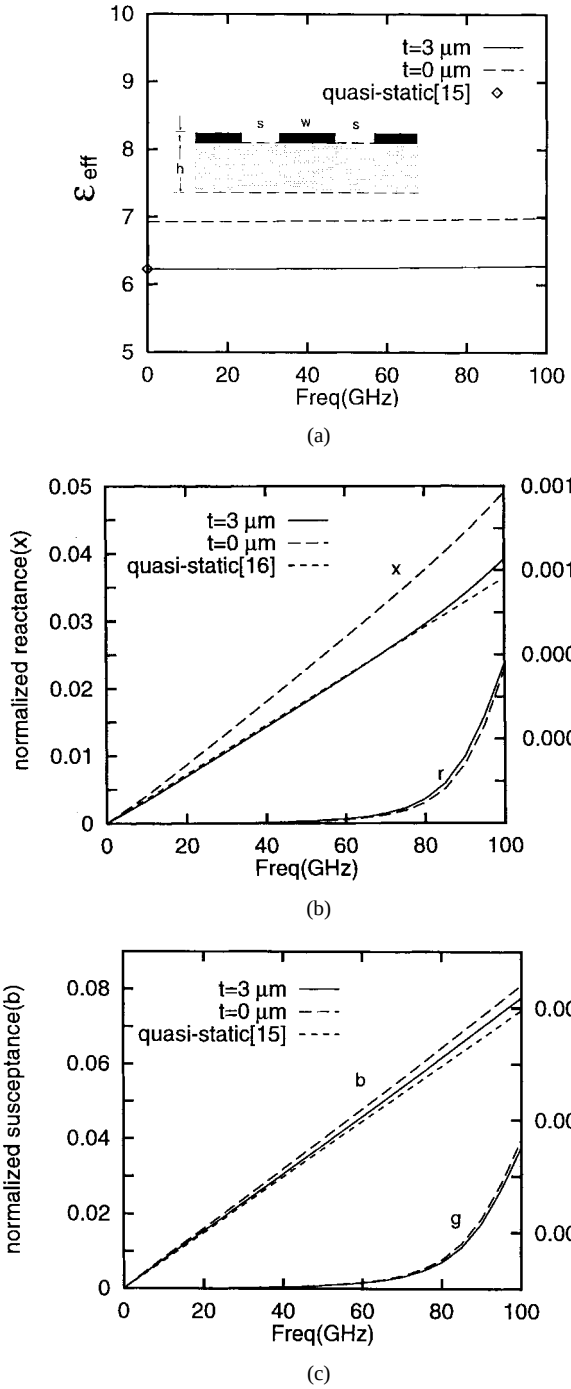


Fig. 4. (a) Effective dielectric constants of uniform CPW. (b) The normalized short-end resistances and reactances, and (c) the normalized open-end conductances and susceptances versus frequency.

in which the $S_{11}$ is extracted by the matrix pencil approach [19]. For comparison, the inductance value calculated in quasi-static approximation for $t = 3$ $\mu$m are included [16]. Fig. 4(c) shows the normalized conductances and susceptances of a CPW open end, where the normalized admittance is calculated from

$$y = g + jb = \frac{1 - S_{11}}{1 + S_{11}} \tag{18}$$

Also, the capacitance value calculated in quasi-static approximation for $t = 3$ $\mu$m are included [15].

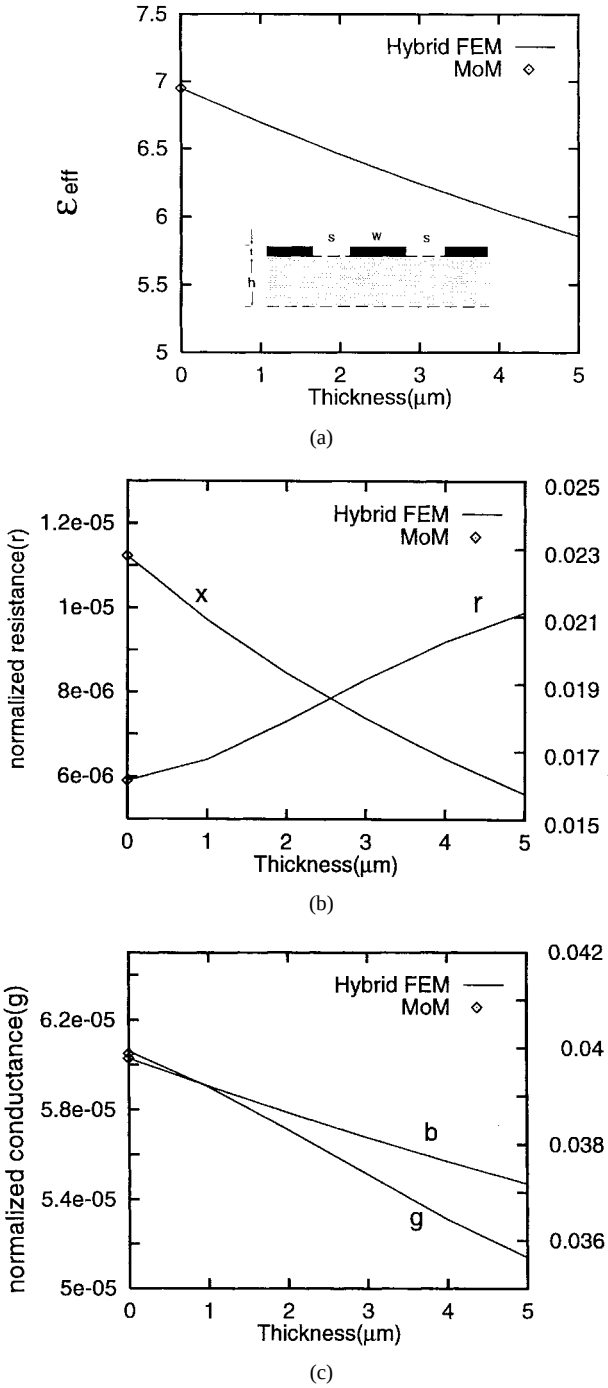


Fig. 5. (a) Effective dielectric constant of uniform CPW. (b) The normalized short-end resistances and reactances, and (c) normalized open-end conductances and susceptances versus metallization thickness $t$ ($f = 50$ GHz).

The influence of metallization thickness on the circuit parameters by the present approach is investigated next. Here the frequency is fixed at 50 GHz. The results in the limiting case of zero metallization thickness are calculated by the moment method. Fig. 5(a) shows the effect of metallization thickness on the effective dielectric constant of a uniform CPW. As expected, the effective dielectric constant decreases as the conductor thickness increases, since comparatively more fields are in the free-space slot region. Fig. 5(b) and (c) show the normalized short-end impedances and open-end admittances, respectively, versus the conductor thickness.

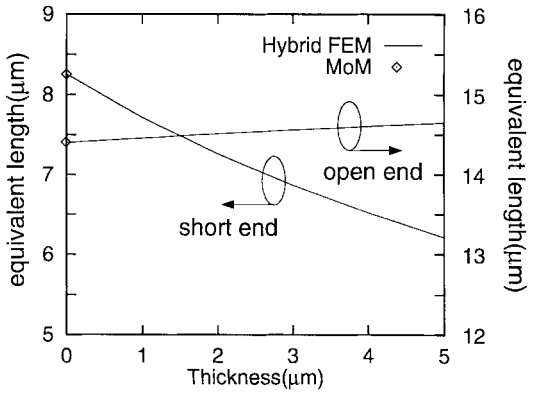


Fig. 6. The equivalent length extensions of the short and open circuits versus metallization thickness $t$ ($f = 50$ GHz).

Please notice the extremely small resistance or conductance at this high frequency, which justifies the applicability of the quasi-static analysis [15], [16].

Fig. 6 shows the dependence of the equivalent extension length on metallization thickness for both short and open ends. The equivalent extension lengths are determined from the normalized reactance and susceptance by the following:

$$x = \frac{\omega L_{\mathrm{CPW}}^{\mathrm{end}}}{Z_o} = \tan(\beta \Delta l_{\mathrm{eq}}) \approx \beta \Delta l_{\mathrm{eq}}, \qquad \text{for short end}$$

$$b = \frac{\omega C_{\mathrm{CPW}}^{\mathrm{end}}}{Y_o} = \tan(\beta \Delta l_{\mathrm{eq}}) \approx \beta \Delta l_{\mathrm{eq}}, \qquad \text{for open end.}$$

As expected, when the thickness of the conductor tends to zero, the results calculated by the present approach move toward the values obtained by the moment method in zero thickness case. It is worth mentioning that the equivalent extension length of the CPW short end decreases as the metallization thickness increases. Comparatively, the equivalent extension length of the CPW open end is almost independent of the metallization thickness.

## V. Consideration of Conductor Profile Effect

As with the development of submicron IC technology, the dimension of a MMIC can be substantially shrunken. As a result, the effects of conductor thickness and conductor-edge profile cannot be ignored due to the narrower slot aperture of the CPW. Fig. 7 shows the cross section of the CPW with two kinds of trapezoidal conductor strips. Fig. 7(a) simulates the profile by underetching and Fig. 7(b) simulates electrolytical growth in the fabrication process, respectively. The trapezoidal shape is defined by the edge angle $\alpha$. The dimension parameters $s$, $w$, and $g$ now denote the average slot width, strip width, and gap width, respectively, which are measured at the plane parallel to, and equally separated from, the upper and bottom surfaces $S_u$ and $S_l$.

Due to the flexibility of the FEM, arbitrary conductor cross section can be easily manipulated, as in the case of rectangular conductor cross section. All we have to do is to replace the rectangular brick element by the hexahedral element shown in Fig. 7(c). The edge vector basis functions and the involved element integrations are well documented in [22]. It deserves

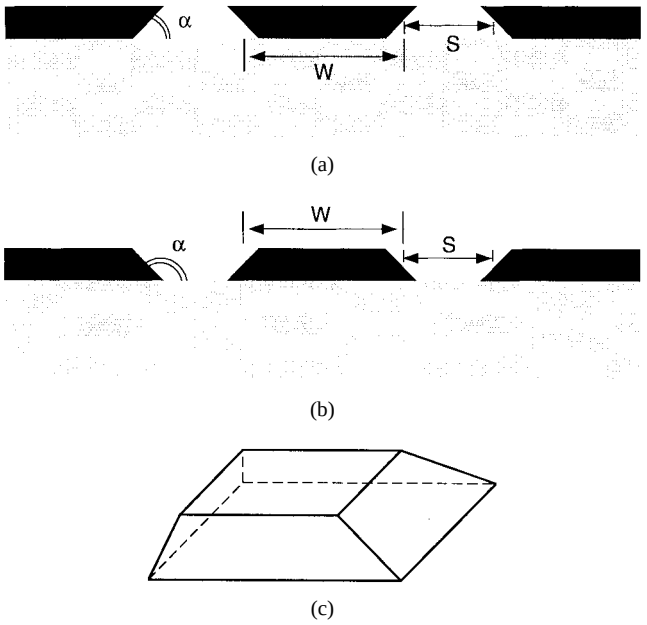


Fig. 7. The cross-sectional geometry of the CPW with trapezoidal conductor cross section. (a) $\alpha = 45°$, (b) $\alpha = 135°$, and (c) hexahedral edge element.

mentioning that the associated patches in the top and bottom surfaces retain rectangular shapes and, hence, no additional efforts are required in evaluating the boundary terms. For the first time, CPW short- and open-ended discontinuities with trapezoidal metallization cross section are calculated.

Fig. 8(a) shows the effects of conductor-edge profile of the CPW on the effective dielectric constants which are extracted from the full-wave analysis of a CPW short end. Here, the average slot width $s$ and strip width $w$ are fixed at 15 and 20 $\mu$m, respectively. The case of $\alpha = 90°$ corresponds to the rectangular conductor cross section. It can be found that the effective dielectric constant in case of $\alpha = 45°$ is smaller than that of the rectangular conductor cross section. This is expected since the fields are more concentrated in the air region due to the sharp edge at top surface of strip. The results of $\alpha = 135°$ are opposite to those of $\alpha = 45°$, since the fields are more concentrated in the substrate region due to the sharp edge at the bottom surface of strip. Fig. 8(b) and (c) show the results of the normalized short-end impedances and open-end admittances versus frequency for the three different cases. For open-end discontinuity, the equivalent capacitance increases as the edge angle $\alpha$ becomes larger. However, the equivalent inductance of the short-end discontinuity decreases as the cross section deviates from the rectangular shape.

Fig. 9 shows the dependence of some circuit parameters on the metallization thickness with edge angle $\alpha$ as a parameter. The current parameter of interest shown in Fig. 9(a) is the effective dielectric constant. The thicker the metallization is, the more significant influence the edge angle exhibits. Fig. 9(b) presents the equivalent length of short- and open-ended CPW discontinuities. For the CPW short end, it can be found that the results of $\alpha = 45°$ are similar to those of $\alpha = 135°$. The reason is that the equivalent end inductances are mainly dependent on the conductors, being almost independent of the dielectric medium in the substrate. In contrast, the substrate

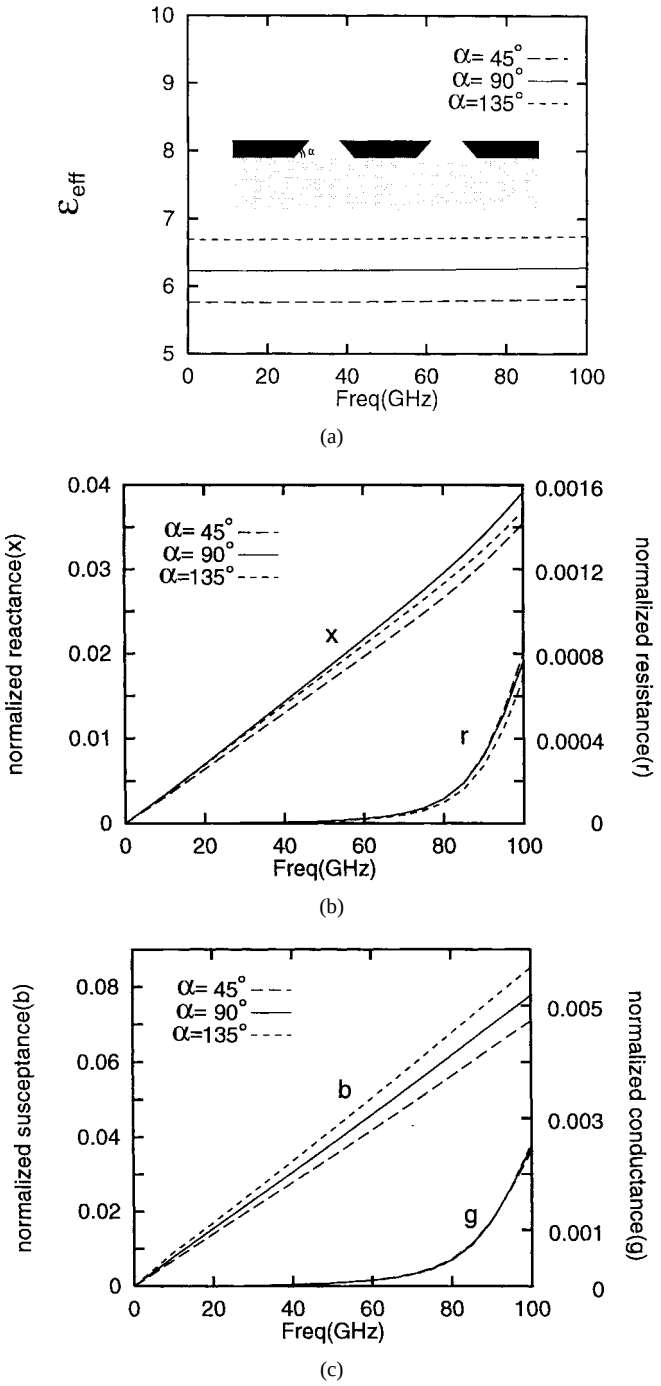


Fig. 8. (a) Effective dielectric constants of uniform CPW. (b) The normalized short-end resistances and reactances, and (c) the normalized open-end conductances and susceptances versus frequency with edge angle $\alpha$ as a parameter.

has a strong influence on the electric field, which determines the capacitances. It can be found that the equivalent length extension for the CPW open-ended discontinuity exhibits different behaviors for $\alpha = 45°$ and $\alpha = 135°$.

## VI. Conclusions

An analysis has been presented to handle the CPW of finite-metallization thickness with rectangular or trapezoidal cross sections. The variational-reaction theory is utilized to

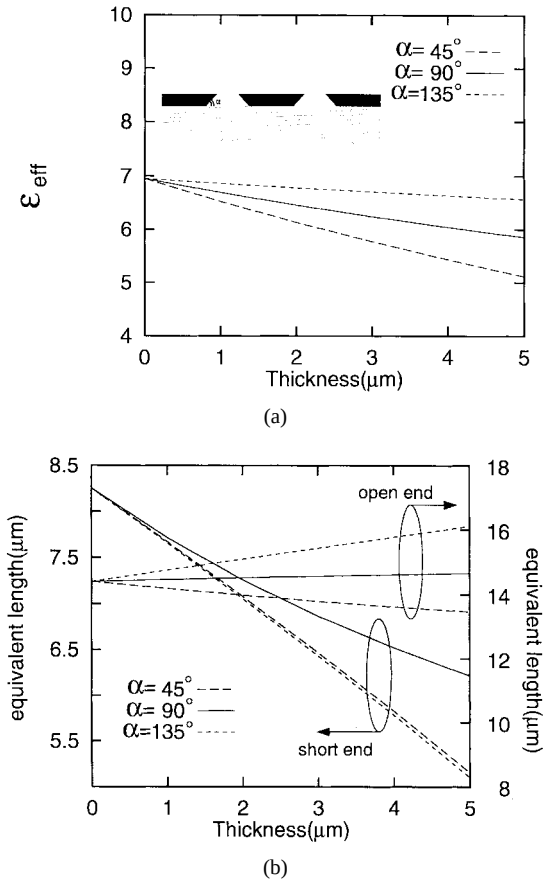


Fig. 9. (a) Effective dielectric constants of uniform CPW, and (b) the equivalent length extensions of the short and open circuits versus metallization thickness $t$ with edge angle $\alpha$ as a parameter ($f = 50$ GHz).

derive a variational equation and the FEM is employed to discretize this equation into a matrix form. In the limiting case of zero metallization thickness, the analysis is reduced to a moment-method analysis using Galerkin's approach with rooftop basis functions. Surface-wave and radiation effects are included in the integral equation formulation in terms of suitable Green's functions. The present analysis can successfully analyze the effects of conductor thickness as well as nonrectangular conductor cross section on the CPW discontinuities for the first time. It has been applied to investigate the effective dielectric constants of CPW lines, as well as the equivalent circuit parameters of the short- and open-ended discontinuities. Numerical results have shown that these effects must be accounted for in order to obtain accurate and reliable predictions of the circuit performance for MMIC applications.

## REFERENCES

[1] C. W. Kuo and T. Itoh, "Characterization of shielded coplanar type transmission line junction discontinuities incorporating the finite metallization thickness effect," *IEEE Trans. Microwave Theory Tech.*, vol. 40, pp. 73–80, Jan. 1992.

[2] T. W. Huang and T. Itoh, "The influence of metallization thickness on the characteristics of cascaded junction discontinuities of shielded coplanar type transmission line," *IEEE Trans. Microwave Theory Tech.*, vol. 41, pp. 693–697, Apr. 1993.

[3] R. Schmidt and P. Russer, "Modeling of cascaded coplanar waveguide discontinuities by the mode-matching approach," in *IEEE MTT-S Int. Microwave Symp. Dig.*, Orlando, FL, May 1995, pp. 281–284.

[4] W. Menzel and W. Grabherr, "Coplanar waveguide short circuit with finite metallization thickness," in *Proc. European Microwave Conf.*, Budapest, Hungary, Sept. 1990, pp. 1187–1192.

[5] F. Alessandri, G. Baini, M. Mongiardo, and R. Sorrentino. "A 3-D mode matching technique for the efficient analysis of coplanar MMIC discontinuities with finite metallization thickness," *IEEE Trans. Microwave Theory Tech.*, vol. 41, pp. 1625–1629, Sept. 1993.

[6] K. Beilenhoff, H. Klingbeil, W. Heinrich, and H. L. Hartnagel, "Open and short circuits in coplanar MMIC's," *IEEE Trans. Microwave Theory Tech.*, vol. 41, pp. 1534–1537, Sept. 1993.

[7] A. M. Tran and T. Itoh, "Full-wave modeling of coplanar waveguide discontinuities with finite conductor thickness," *IEEE Trans. Microwave Theory Tech.*, vol. 41, pp. 1611–1615, Sept. 1993.

[8] W. Schroeder and I. Wolff, "A new hybrid mode boundary integral method for analysis of MMIC waveguides with complicated cross-section," in *IEEE MTT-S Int. Microwave Symp. Dig.*, Long Beach, CA, June 1989, pp. 711–714.

[9] K. A. Michalski and D. Zheng, "Rigorous analysis of open microstrip lines of arbitrary cross section in bound and leaky regimes," *IEEE Trans. Microwave Theory Tech.*, vol. 37, pp. 2005–2010, Dec. 1989.

[10] C. J. Railton and J. P. McGeehan, "An analysis of microstrip with rectangular and trapezoidal conductor cross sections," *IEEE Trans. Microwave Theory Tech.*, vol. 38, pp. 1017–1022, Aug. 1990.

[11] F. Olyslager, D. De Zutter, and K. Blomme, "Rigorous analysis of the propagation characteristics of general lossless and lossy multiconductor transmission lines in multilayered media," *IEEE Trans. Microwave Theory Tech.*, vol. 41, pp. 79–88, Jan. 1993.

[12] M. S. Alam, K. Hirayama, Y. Hayashi, and M. Koshiba, "Analysis of shielded microstrip lines with arbitrary metallization cross section using a vector finite element method," *IEEE Trans. Microwave Theory Tech.*, vol. 42, pp. 2112–2117, Nov. 1994.

[13] Z. Ma, E. Yamashita, and S. Xu, "Hybrid-mode analysis of planar transmission lines with arbitrary metallization cross sections," *IEEE Trans. Microwave Theory Tech.*, vol. 41, pp. 491–497, Mar. 1993.

[14] L. Zhu and E. Yamashita, "Effects of conductor edge profile on transmission properties of conductor-backed coplanar waveguides," *IEEE Trans. Microwave Theory Tech.*, vol. 43, pp. 847–853, Apr. 1995.

[15] C. W. Chiu and R. B. Wu, "Capacitance computation for CPW discontinuities with finite metallization thickness by hybrid finite element method," *IEEE Trans. Microwave Theory Tech.*, vol. 45, pp. 498–504, Apr. 1997.

[16] ———, "Inductance computation for CPW discontinuities with finite metallization thickness by hybrid finite element method," *IEEE Trans. Microwave Theory Tech.*, private communication.

[17] R. B. Wu and C. H. Chen, "On the variational reaction theory for dielectric waveguides," *IEEE Trans. Microwave Theory Tech.*, vol. MTT-33, pp. 576–583, June 1985.

[18] C. G. Jan, R. B. Wu, P. Hsu, and D. C. Chang, "Analysis of edge slots in rectangular waveguide with finite waveguide wall thickness," *IEEE Trans. Antennas Propagat.*, vol. 44, pp. 1120–1126, Aug. 1996.

[19] M. D. Wu, S. M. Deng, R. B. Wu, and P. Hsu, "Full-wave characterization of mode conversion in a coplanar waveguide right-angled bend," *IEEE Trans. Microwave Theory Tech.*, vol. 43, pp. 2532–2538, Nov. 1995.

[20] K. Ise, K. Inoue, and M. Koshiba, "Three-dimensional finite-element method with edge-elements for electromagnetic waveguide discontinuities," *IEEE Trans. Microwave Theory Tech.*, vol. 39, pp. 1289–1295, Aug. 1991.

[21] J. Bornemmann, "A scattering-type transverse resonance technique for the calculation of (M)MIC transmission line characteristics," *IEEE Trans. Microwave Theory Tech.*, vol. 39, pp. 2083–2088, Dec. 1991.

[22] J. M. Jin, *The Finite Element Method in Electromagnetics.* New York: Wiley, 1993, ch. 8.

**Fang-Lih Lin** was born in Yunlin, Taiwan, R.O.C., in 1969. He received the B.S. degree in electronic engineering from National Chiao-Tung University, Hsin-Chu, Taiwan, R.O.C., in 1992, and the M.S. degree in electrical engineering from National Taiwan University, Taipei, Taiwan, R.O.C., in 1994, where he is currently working toward the Ph.D. degree.

His current research interests include transmission-line discontinuity, analysis, and design of microwave circuit.

**Ruey-Beei Wu** (M'91) was born in Tainan, Taiwan, R.O.C., in 1957. He received the B.S.E.E. and Ph.D. degrees from National Taiwan University, Taipei, Taiwan, R.O.C., in 1979 and 1985, respectively.

In 1982, he joined the faculty of the Department of Electrical Engineering, National Taiwan University, where he is currently a Professor. From March 1986 to February 1997, he was a Visiting Scholar at the IBM East Fishkill Facility, NY. From August 1994 to July 1995, he was with the Electrical Engineering Department, University of California at Los Angeles. His areas of interest include computational electromagnetics, dielectric waveguides, edge slot antennas, wave scattering of composite materials, transmission line and waveguide discontinuities, and interconnection modeling for computer packaging.